

# Qubit-efficient quantum combinatorial optimization solver

Bhuvanesh Sundar\* and Maxime Dupont

Rigetti Computing, 775 Heinz Avenue, Berkeley, California 94710, USA

Quantum optimization solvers typically rely on one-variable-to-one-qubit mapping. However, the low qubit count on current quantum computers is a major obstacle in competing against classical methods. Here, we develop a qubit-efficient algorithm that overcomes this limitation by mapping a candidate bit string solution to an entangled wave function of fewer qubits. We propose a variational quantum circuit generalizing the quantum approximate optimization ansatz (QAOA). Extremizing the ansatz for Sherrington-Kirkpatrick spin glass problems, we show valuable properties such as the concentration of ansatz parameters and derive performance guarantees. This approach could benefit near-term intermediate-scale and future fault-tolerant small-scale quantum devices.

An ongoing effort in quantum computing seeks to practically demonstrate quantum utility for solving combinatorial optimization problems. Achieving quantum utility could have a significant impact in areas which heavily utilize optimization, such as logistics and supply chains. To this end, various quantum algorithms have been developed and implemented, including annealing approaches [1, 2], parameterized quantum algorithms with variational optimization [3–6], recursive techniques [7–9], and others inspired by leading classical approaches [10, 11].

Quantum algorithms typically map each of the problem variables onto individual qubits and recast the original optimization problem as the ground state search for a Hamiltonian. One of the obstacles in demonstrating quantum utility is the size of the problems one can address, given that current gate-based quantum computers typically have tens to hundreds of qubits [9, 12–19], and quantum annealers have thousands of qubits [2] [20]. Indeed, real-world problems typically have several thousands of variables, which can be handled by classical solvers better than quantum solvers today. A prevailing practical challenge in adding more qubits to the computers is hardware noise, which limits their solution quality. In the absence of quantum error correction [21], more qubits generally means larger and therefore noisier quantum programs, compounding towards a deteriorating output. Meanwhile, initial error-corrected quantum computers are expected to have fewer logical qubits than necessary for quantum utility in optimization. Therefore, qubit-efficient methods for optimization problems could benefit near-term intermediate scale quantum devices as well as fault-tolerant small-scale quantum computers [22–25].

Several qubit-efficient methods have been proposed to overcome the size of current quantum computers. Some of these are generic methods to break down a large quantum circuit into an equivalent set of smaller quantum circuits that can be executed on current devices [26–30], and have been used to solve large optimization problems with more variables than qubits [31, 32]—at the expense of large computational time overheads in classical

or quantum resources. Some approaches, specific to combinatorial optimization, employ decompositions which stitch together an approximate solution for a large optimization problem by solving smaller subproblems [33–35], and again suffer from large overheads induced by the decomposition. Other strategies employ nontrivial mappings between classical variables of the optimization problem and qubits on the device, such as amplitude encoding [36–38], correlation encoding [39], and multibasis encodings [40], each with some challenges for quantum utility. For instance, the amplitude encoding strategy is classically simulatable, while the other strategies use hardware-native variational circuits which may be difficult to optimize [41, 42].

Here, we develop a qubit-efficient encoding based on a many-to-one mapping from variables to qubits. In this approach, classical bitstrings are encoded as entangled wave functions of fewer qubits. In addition, we physically motivate a variational quantum circuit for this encoding, inspired by the quantum approximate optimization algorithm (QAOA) [3]. While the QAOA uses  $q = N$  qubits to store  $N$  variables [3], the proposed algorithm makes the number of qubits  $q$  a tunable parameter. Compared to the overhead of previous decomposition methods [26–35], this algorithm only introduces a polynomial overhead in  $Np$  over the QAOA for  $p$  layers. We show that this algorithm has several properties also present in the QAOA, such as parameter clustering and performance guarantees for some classes of problems [43–46]. We numerically benchmark the algorithm for Sherrington-Kirkpatrick (SK) spin glass models [47] and test it on Rigetti’s Ankaa<sup>TM</sup>-9Q-3 superconducting chip.

*Qubit-efficient encoding.*— Given  $N$  binary variables  $\mathbf{z} = (z_1, \dots, z_N)$ , we divide the variables into  $N/d$  groups of  $d$  variables each, as shown in Fig. 1(a), and denote each group with a label  $\ell$  which runs from 0 to  $N/d - 1$ . Without loss of generality, we assume  $N$  is divisible by  $d$ .  $d$  may be chosen by the user, for example depending on the number of available qubits or the desired algorithm performance as described later. The variables are stored in an entangled wave function  $|\phi(\mathbf{z})\rangle$  of  $q = d + \log_2(N/d)$

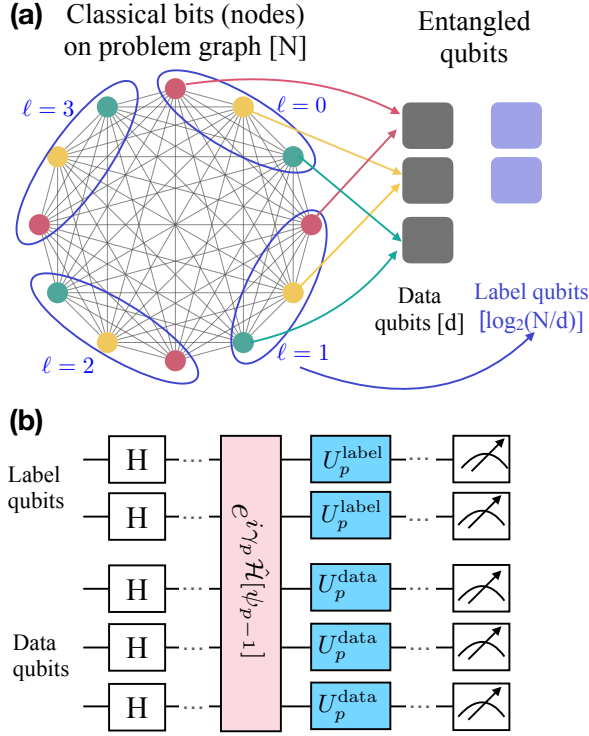


FIG. 1. (a) Qubit-efficient encoding of variables onto qubits via a many-to-one mapping from variables to qubits. Graph nodes, which host variables, are color-coded for convenience. All nodes with the same color are mapped to the same *data* qubit (in grey). The value of the *label* qubits (purple) dictates which node is stored in the data qubit. Links between nodes represent interactions between nodes in the optimization problem [see text]. (b) Parameterized quantum circuit to solve combinatorial optimization problems with qubit-efficient encoding. The circuit consists of an initial layer of Hadamard gates, followed by alternating layers of entangling ( $e^{i\gamma_p \hat{H}}$ ) and one-qubit gates ( $U_p$ ). The entangling gates in the  $p$ th layer is determined from measurements of the wave function at the end of the  $(p-1)$ th layer. The parametric angles are chosen classically to minimize the cost measured by the quantum computer.

qubits as

$$|\phi(\mathbf{z})\rangle \equiv \sum_{\ell=0}^{N/d-1} \lambda_{\ell} |\ell\rangle_{\text{label}} \otimes |\mathbf{z}_{\ell}\rangle_{\text{data}}, \quad (1)$$

where  $|\ell\rangle$  is the  $\log_2(N/d)$ -qubit product state in the binary representation for  $\ell$ ,  $|\mathbf{z}_{\ell}\rangle \equiv |z_{(N/d-1)\ell+1}, z_{(N/d-1)\ell+2}, \dots, z_{(N/d)\ell}\rangle$  stores  $d$  binary variables, and  $\lambda_{\ell}$  are arbitrary complex coefficients with  $\sum_{\ell} |\lambda_{\ell}|^2 = 1$ . This wave function stores all  $N$  binary variables of  $\mathbf{z}$ , and a single projective measurement gives the values of  $d$  variables,  $\mathbf{z}_{\ell} \equiv (z_{(N/d-1)\ell+1}, z_{(N/d-1)\ell+2}, \dots, z_{(N/d)\ell})$ , read from the *data* qubits conditioned on measuring the *label* qubits in  $\ell$ . For convenience, we denote  $\ell_i \equiv \lfloor \frac{i}{d} \rfloor$  as the label value for the variable  $z_i$ , and  $d_i \equiv i \bmod d$  as the data qubit which stores  $z_i$  conditioned on the label

qubits' state being  $|\ell_i\rangle$ .

Figure 1(a) shows an example of the qubit-efficient encoding with  $N = 12, d = 3$ . All variables  $z_i$  with the same data qubit  $d_i$  are given the same color, for convenience of visualization. All variables within a blue ellipse are given the same label  $\ell$ . In this case, the 12 variables are stored in 5 qubits.

In the case of  $d = N$ ,  $|\phi(\mathbf{z})\rangle \equiv |z_1, z_2, \dots, z_N\rangle_{\text{data}}$  reduces to the usual way of storing binary variables in a product state of the qubits. Nearly all the literature up to now for solving optimization problems considered  $d = N$  [4, 5]. For  $d < N$ , the wave function stores the variables using a  $(N/d)$ -to-one map between the variables and data qubits. This encoding describes a generic method to efficiently store classical binary variables in qubits.

The case of  $d = 1$ , first proposed in [48] and further explored in [49–52] using a hardware-native ansatz, is notable since it requires only  $1 + \log_2(N)$  qubits to store  $N$  binary variables. However, we note that quantum circuits in this case can be classically simulated in time scaling as  $O(Np)$  where  $p$  parametrizes the circuit depth (see below), and similarly for  $d \lesssim \log_2 N$ . Under the widely held belief that quantum algorithms may not be able to achieve exponential speedup for NP-hard problems, it is unclear where the difficulty for the quantum algorithms at  $d \lesssim \log_2 N$  lies, with potential candidates being a large circuit depth  $p$  or expensive computational time for parameter search.

The main aim of this paper is to develop a quantum algorithm that uses qubit-efficient encoding to solve combinatorial optimization problems, and investigate the cases with  $1 \leq d \leq N$ .

*Binary optimization problem.*– Binary optimization problems seek to minimize a cost function  $C(\mathbf{z})$  of variables  $\mathbf{z} = (z_1, \dots, z_N)$  with  $z_i \in \{\pm 1\}$ , where the function  $C$  is generically written as a polynomial in the variables, e.g.,  $C = \sum_i w_i z_i + \sum_{ij} w_{ij} z_i z_j + \dots$ . To develop a quantum algorithm that minimizes this cost, one should express the cost as expectation value(s) with respect to samples from the wave function  $|\psi\rangle$ . This task is trivial for  $d = N$ , but nontrivial for  $d < N$ .

For simplicity, let us consider one of the singleton terms in the cost,  $w_i z_i$ . Since the value of the variable  $z_i$  can be obtained only when the label bits are measured as  $\ell_i$ , an estimation  $\bar{z}_i$  for this variable is obtained from averaging the shot values of the Pauli operator  $\hat{Z}_{d_i}$ , post-selecting only those measurements with the label bits as  $\ell_i$ . This can be written as the conditional expectation value,

$$\bar{z}_i = \frac{\langle \psi | \hat{P}_{\ell_i} \hat{Z}_{d_i} | \psi \rangle}{\langle \psi | \hat{P}_{\ell_i} | \psi \rangle}, \quad (2)$$

where  $\hat{P}_{\ell} = |\ell\rangle_{\text{label}} \langle \ell|_{\text{label}}$  is a projection operator. Similarly, for variables  $z_i$  and  $z_j$  with the same label,  $\ell_i = \ell_j$ ,  $z_i z_j$  can be estimated by post-selecting on shots where

the label bits were  $\ell_i$ , therefore the estimate  $\overline{z_i z_j}$  is

$$(\overline{z_i z_j})_{\ell_i = \ell_j} = \frac{\langle \psi | \hat{P}_{\ell_i} \hat{Z}_{d_i} \hat{Z}_{d_j} | \psi \rangle}{\langle \psi | \hat{P}_{\ell_i} | \psi \rangle}. \quad (3)$$

If  $\ell_i \neq \ell_j$ ,  $z_i$  and  $z_j$  are never measured together in the same shot, therefore we estimate  $\overline{z_i z_j}$  as  $\bar{z}_i \times \bar{z}_j$ . In this way, quadratic terms of the form  $C(\mathbf{z}) = \sum_{i < j} w_{ij} z_i z_j$ , for example, can be expressed as

$$C[\psi] = \sum_{\substack{i < j \\ \ell_i = \ell_j}} w_{ij} \overline{z_i z_j} + \sum_{\substack{i < j \\ \ell_i \neq \ell_j}} w_{ij} \bar{z}_i \bar{z}_j. \quad (4)$$

This construction can be straightforwardly extended to measure any polynomial in  $\mathbf{z}$ .

The cost in Eq. (4) can be written as  $C[\psi] = \langle \psi | \hat{\mathcal{H}}[\psi] | \psi \rangle$  with

$$\begin{aligned} \hat{\mathcal{H}}[\psi] = & \sum_{\substack{i < j \\ \ell_i = \ell_j}} w_{ij} \frac{\hat{P}_{\ell_i} \hat{Z}_{d_i} \hat{Z}_{d_j}}{\langle \psi | \hat{P}_{\ell_i} | \psi \rangle} \\ & + \frac{1}{2} \sum_{\substack{i < j \\ \ell_i \neq \ell_j}} w_{ij} \left( \bar{z}_i \frac{\hat{P}_{\ell_j} \hat{Z}_{d_j}}{\langle \psi | \hat{P}_{\ell_j} | \psi \rangle} + \bar{z}_j \frac{\hat{P}_{\ell_i} \hat{Z}_{d_i}}{\langle \psi | \hat{P}_{\ell_i} | \psi \rangle} \right). \end{aligned} \quad (5)$$

We highlight that the Hamiltonian  $\hat{\mathcal{H}}[\psi]$  depends on  $|\psi\rangle$ , a consequence of the cost being nonlinear in  $|\psi\rangle \langle \psi|$ . The first line in Eq. (5) describes interactions between nodes with the same group, and the second line in Eq. (5) describes interactions between nodes in different groups.

This construction of  $\hat{\mathcal{H}}$  and  $C$  smoothly connects in the  $d = N$  limit with their standard forms in the QAOA,  $\hat{\mathcal{H}} = \sum_i w_i \hat{Z}_i + \sum_{i,j} w_{ij} \hat{Z}_i \hat{Z}_j + \dots$  and  $C = \langle \hat{\mathcal{H}} \rangle$ . Therefore many known properties of the QAOA may be expected to hold for values of  $d$  close to  $N$  as well, as exemplified later.

Here, we restrict our attention to SK models [47], which have quadratic cost functions of the form of Eq. (4) with fully connected random weights  $w_{ij}$  precisely defined later. Optimization problems expressed as fully connected graphs are ubiquitous in statistical mechanics and computer science [53].

*Ansatz.*— The QAOA ansatz for extremizing  $C$  is  $|\psi_p\rangle = e^{i\beta_p \hat{\mathcal{H}}_x} e^{i\gamma_p \hat{\mathcal{H}}} |\psi_{p-1}\rangle$  [3]. A natural extension of this ansatz generalizes  $\hat{\mathcal{H}}$  to  $\hat{\mathcal{H}}[\psi_{p-1}]$ . Here,  $\hat{\mathcal{H}}_x = \sum_{i=1}^q \hat{X}_i$  is the transverse field mixer Hamiltonian, and  $\hat{\mathcal{H}}[\psi_{p-1}]$  is the layer-dependent cost Hamiltonian, which depends on the wavefunction  $|\psi_{p-1}\rangle$  in the previous layer.

The ansatz is drawn in Fig. 1(b). Determining the cost Hamiltonian in the  $p$ th layer,  $\hat{\mathcal{H}}[\psi_{p-1}]$ , requires to first know  $\bar{\mathbf{z}}$  and  $\langle \psi_{p-1} | \hat{P}_{\ell} | \psi_{p-1} \rangle$ , which can be obtained from projective measurements after  $p-1$  layers. Circuit implementation of  $\exp(i\gamma \hat{\mathcal{H}})$  is discussed in [54]. Below, we exemplify this ansatz using a SK problem instance, and argue for a slight modification to the ansatz.

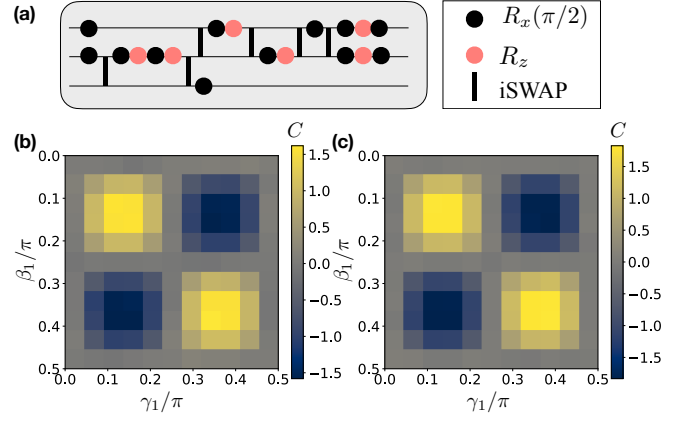


FIG. 2. (a) Schematic of quantum circuit that implements a  $p = 1$  layer of the ansatz, for a  $N = 4$  SK model instance at  $d = 2$ . Orange and black dots are  $R_x$  and  $R_z$  gates, and vertical lines are iSWAPs [54]. (b-c) Cost landscape for the ansatz versus  $\beta_1$  and  $\gamma_1$ , measured from experiments on Rigetti's Ankaa™-9Q-3 chip, and numerically computed from an ideal simulation of the circuit, with 10000 shots.

*N=4 example.*— We consider a SK model problem with  $N = 4$  variables, where the weights  $w_{ij}$  are chosen randomly from  $\{\pm 1\}$ . The model weights for the specific instance are given in [54]. For this example, we encode the problem on 3 qubits using  $d = 2$ . Figure 2(a) shows the circuit required to implement the ansatz at  $p = 1$ , expressed in terms of quantum gates native to Rigetti's Ankaa™-9Q-3 superconducting quantum chip (see [54] for definitions of these gates, and a circuit compilation of the ansatz).

Figures 2(b-c) plot the cost yielded by the ansatz versus  $\beta_1$  and  $\gamma_1$ , with results measured on Rigetti's Ankaa™-9Q-3 in (b), and numerically obtained from a noiseless simulator in (c). We find extremely good agreement between the landscapes, with a Pearson correlation coefficient of 0.997. There is a small  $\sim 15\%$  scale reduction of the cost on Ankaa™-9Q-3, that is attributable to hardware noise. However, the  $p = 1$  ansatz does not produce the ground state cost (see [54]), and *cannot* produce the ground state cost at any  $p$  due to a symmetry explained below.

The SK problem instance has two degenerate solutions,  $\mathbf{z}^*$  and  $-\mathbf{z}^*$ , due to a global  $\mathbb{Z}_2$  spin-flip symmetry. Similarly, the ansatz also has a global spin-flip symmetry for the data qubits. The ansatz at  $p = 1$  and the optimal angles [54] prepares an equal superposition of the two ground state solutions  $\mathbf{z}^*$  and  $-\mathbf{z}^*$ , i.e.  $|\psi_{p=1}\rangle = (|\phi(\mathbf{z}^*)\rangle + |\phi(-\mathbf{z}^*)\rangle)/\sqrt{2}$ . Yet, since  $\bar{z}_i = 0 \forall i$  due to the spin-flip symmetry (see [54]), the ansatz fails to produce the minimum cost. We note that this is unique to the qubit-efficient encoding, and does not occur at  $d = N$ .

Thus, breaking the  $\mathbb{Z}_2$  symmetry of the ansatz is needed to produce the ground state cost. Therefore, we

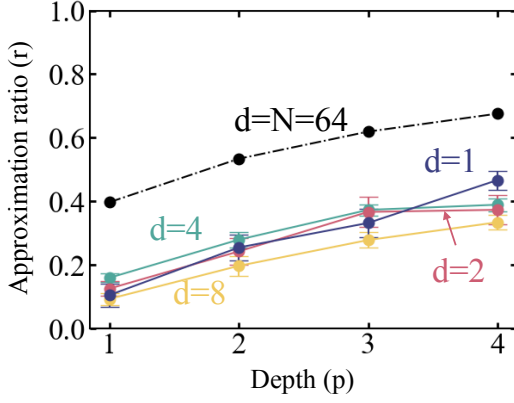


FIG. 3. Average approximation ratios produced by the optimal circuits in Fig. 1(b), for ensemble of five Sherrington-Kirkpatrick spin glass model problems with  $N = 64$  variables and  $w_{ij} \in \{\pm 1\}$ , at various values of  $d$ .

modify the ansatz to

$$|\psi_p\rangle = e^{i\beta_p \hat{\mathcal{H}}_x} e^{i\gamma'_p \hat{\mathcal{H}}_z} e^{i\gamma_p \hat{\mathcal{H}}[\psi_{p-1}]} |\psi_{p-1}\rangle, \quad (6)$$

where  $\hat{\mathcal{H}}_z = \sum_{i \in \text{data}} \hat{Z}_i$  describes one-body bias terms.

*Variational optimization.*— We illustrate the performance of the symmetry-broken ansatz using an ensemble of SK problem instances at  $N = 64$  and  $128$  with  $w_{ij} \in \{\pm 1\}$ . We optimize the  $(\beta_i, \gamma_i, \gamma'_i)$  parameters in the ansatz with a classical optimizer which seeks to minimize  $C[\psi_p]$ . We use a basin-hopping optimizer [55] with L-BFGS-B as the local optimization method [56]. To benchmark the cost produced by variational optimization, we compare it against the ground state cost  $C^*$  found with a classical heuristic algorithm based on tabu search [57] implemented in MQLib [58].

In Fig. 3, we plot the optimized approximation ratios,  $r = C/C^*$ , averaged over an ensemble of five SK problems with  $N = 64$  variables, using different values of  $d < N$ . The dashed line at  $d = N$  is plotted using values predicted in Ref. [43] for large  $N$ . Our ansatz at  $d < N, p = 3$  produces results comparable to the ansatz at  $d = N, p = 1$ , despite having up to 9 times fewer qubits at  $d = 1$ . Similarly, the ansatz at  $d = 1, p = 4$  produces results similar to the ansatz at  $d = N, p = 2$ .

In addition to the quality of the solution produced by an algorithm, the time taken by the algorithm is also an important factor. A significant contributor to the total time of variational quantum algorithms is the time taken to find the optimal parameters. Figure 3 shows no clear distinction in the quality of solution produced by different  $d$  at the same  $p$ . But we argue next that larger values of  $d$  may require lesser parameter search time due to clustering of optimal parameters for SK problem instances.

*Concentration of parameters.*— Previous works have shown empirical and analytical evidence for clustering of optimal parameters in the QAOA ( $d = N$ ) for some

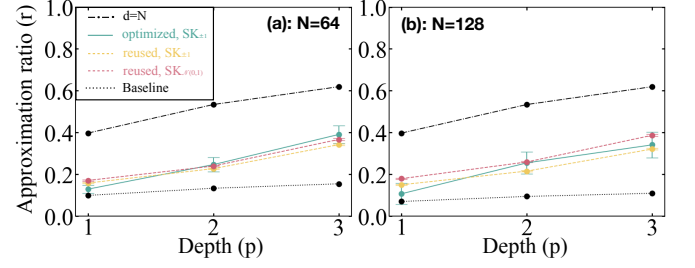


FIG. 4. Average approximation ratios for optimized parameters for five SK problem instances (teal), and for 100 SK problem instances where the same parameters were used for all the instances (yellow and magenta). Instances in yellow have  $w_{ij} = \pm 1$  while magenta instances have  $w_{ij} \sim \mathcal{N}(0, 1)$ . The parameters for the yellow and magenta curves in (b) are related to those of (a) by a trivial rescaling [54].

classes of problems including SK problems [43, 44, 59–62]. It is interesting to ask whether a similar property holds for the qubit-efficient ansatz. Figure 4 demonstrates empirical evidence for parameter concentration for SK problems in the qubit-efficient ansatz. We implemented the ansatz for solving 100 SK problem instances, using the optimized parameters for one of the SK problem instances from Fig. 3. The yellow dashed line in Fig. 4(a) plots the mean  $r$  vs  $p$  for 100 SK problem instances with  $w_{ij} = \pm 1$ , and shows that the mean  $r$  for 100 problem instances closely follows the optimized  $r$  for five problem instances (solid teal curve). Furthermore, the magenta dashed line in Fig. 4(a), which plots the mean approximation ratio for problems with normally distributed weights,  $w_{ij} \sim \mathcal{N}(0, 1)$ , shows evidence that the same parameters obtained from the case with  $w_{ij} \in \{\pm 1\}$  can also be used to solve the ensemble with  $w_{ij} \sim \mathcal{N}(0, 1)$ . Our ansatz beats a baseline performance that comes from a naive problem decomposition method, explained in [54].

Figure 4(b) demonstrates another useful property that near-optimal parameters for  $N > 64$  can be derived from those at  $N = 64$ . We solve SK problems with  $N = 128$ , by reusing the same parameters from the  $N = 64$  case in (a) with a trivial rescaling [54], and still find approximation ratios close to the optimized  $r$  for five problem instances (solid teal curve).

*Outlook.*— We have shown that a QAOA-inspired algorithm for solving SK spin glass problems, with a qubit-efficient encoding scheme which maps many variables to each qubit in a register, achieves an approximation ratio within  $O(1)$  of that of the QAOA, while using substantially fewer qubits. We demonstrated a proof-of-principle experimental benchmark of the algorithm for solving a small SK model problem on Rigetti’s Ankaa<sup>TM</sup>-9Q-3 superconducting chip. We derived a performance guarantee for our ansatz, and showed evidence of parameter clustering at  $d = 4$ , which could significantly alleviate classical resources for parameter optimization. We did



not find parameter concentration at  $d < 4$ , which could indicate one of the difficulties in implementing the algorithm with  $O(\log_2 N)$  qubits, and therefore a preference for larger  $d$ . However, this preference for more qubits should be weighed against the increased hardware noise in the circuit when more qubits are present. Moreover, one should consider the fact that the solution bit string would be stored as an entangled final wave function which may be less robust to noise when more qubits are used. Thus, investigating the optimal value of  $d$  on real hardware would be an interesting question to explore in the future.

Our algorithm can be straightforwardly extended to other classes of combinatorial problems, and is expected to have a trainable QAOA-like ansatz that may have parameter clustering or at least good heuristics for seed parameters, and lesser overheads than standard problem decomposition methods [26–35]. The qubit-efficient scheme may also be applied to other use cases such as quantum machine learning, and is likely to be useful in the near future as we enter the era of small-scale fault-tolerant quantum computers [22–25].

We thank Stuart Hadfield, Mark Hodson, Marco Paini, Alex Place, Matt Reagor, Graham Reid, and Davide Venturelli for valuable discussions. This work is supported by the Defense Advanced Research Projects Agency (DARPA) under Agreement No. HR-0011-23-3-0015. This research used resources of the National Energy Research Scientific Computing Center, a DOE Office of Science User Facility supported by the Office of Science of the U.S. Department of Energy under Contract No. DE-AC02-05CH11231 using NERSC awards DDR-ERCAP0024427 and ASCR-ERCAP0028951. The views, opinions and/or findings expressed are those of the authors and should not be interpreted as representing the official views or policies of the Department of Defense or the U.S. Government.

---

\* [bsundar@rigetti.com](mailto:bsundar@rigetti.com)

- [1] E. Farhi, J. Goldstone, S. Gutmann, and M. Sipser, Quantum computation by adiabatic evolution, [arXiv](#) , [0001106](#) (2000).
- [2] A. D. King, J. Raymond, T. Lanting, R. Harris, A. Zucca, F. Altomare, A. J. Berkley, K. Boothby, S. Ejtemaee, C. Enderud, *et al.*, Quantum critical dynamics in a 5,000-qubit programmable spin glass, *Nature* **617**, 61 (2023).
- [3] E. Farhi, J. Goldstone, and S. Gutmann, A quantum approximate optimization algorithm, [arXiv](#) , [1411.4028](#).
- [4] M. Cerezo, A. Arrasmith, R. Babbush, S. C. Benjamin, S. Endo, K. Fujii, J. R. McClean, K. Mitarai, X. Yuan, L. Cincio, and P. J. Coles, Variational quantum algorithms, *Nat. Rev. Phys.* **3**, 625 (2021).
- [5] K. Blekos, D. Brand, A. Ceschini, C.-H. Chou, R.-H. Li, K. Pandya, and A. Summer, A review on quantum approximate optimization algorithm and its variants, *Phys. Rep.* **1068**, 1 (2024).
- [6] L. Zhu, H. L. Tang, G. S. Barron, F. A. Calderon-Vargas, N. J. Mayhall, E. Barnes, and S. E. Economou, Adaptive quantum approximate optimization algorithm for solving combinatorial problems on a quantum computer, *Phys. Rev. Res.* **4**, 033029 (2022).
- [7] S. Bravyi, A. Kliesch, R. Koenig, and E. Tang, Obstacles to variational quantum optimization from symmetry protection, *Phys. Rev. Lett.* **125**, 260505 (2020).
- [8] L. T. Brady and S. Hadfield, Iterative quantum algorithms for maximum independent set: a tale of low-depth quantum algorithms, [arXiv](#) , [2309.13110](#).
- [9] M. Dupont, B. Evert, M. J. Hodson, B. Sundar, S. Jeffrey, Y. Yamaguchi, D. Feng, F. B. Maciejewski, S. Hadfield, M. S. Alam, *et al.*, Quantum-enhanced greedy combinatorial optimization solver, *Sci. Adv.* **9**, eadi0487 (2023).
- [10] M. Dupont and B. Sundar, Extending relax-and-round combinatorial optimization solvers with quantum correlations, *Phys. Rev. A* **109**, 012429 (2024).
- [11] D. J. Egger, J. Mareček, and S. Woerner, Warm-starting quantum optimization, *Quantum* **5**, 479 (2021).
- [12] M. P. Harrigan, K. J. Sung, M. Neeley, K. J. Satzinger, F. Arute, K. Arya, J. Atalaya, J. C. Bardin, R. Barends, S. Boixo, *et al.*, Quantum approximate optimization of non-planar graph problems on a planar superconducting processor, *Nat. Phys.* **17**, 332 (2021).
- [13] S. Ebadi, A. Keesling, M. Cain, T. T. Wang, H. Levine, D. Bluvstein, G. Semeghini, A. Omran, J.-G. Liu, R. Samajdar, *et al.*, Quantum optimization of maximum independent set using rydberg atom arrays, *Science* **376**, 1209 (2022).
- [14] F. B. Maciejewski, S. Hadfield, B. Hall, M. Hodson, M. Dupont, B. Evert, J. Sud, M. S. Alam, Z. Wang, S. Jeffrey, *et al.*, Design and execution of quantum circuits using tens of superconducting qubits and thousands of gates for dense ising optimization problems, [arXiv](#) , [2308.12423](#).
- [15] R. Shaydulin, C. Li, S. Chakrabarti, M. DeCross, D. Herman, N. Kumar, J. Larson, D. Lykov, P. Minssen, Y. Sun, *et al.*, Evidence of scaling advantage for the quantum approximate optimization algorithm on a classically intractable problem, *Sci. Adv.* **10**, eadm6761 (2024).
- [16] N. Sachdeva, G. S. Harnett, S. Maity, S. Marsh, Y. Wang, A. Winick, R. Dougherty, D. Canuto, Y. Q. Chong, M. Hush, *et al.*, Quantum optimization using a 127-qubit gate-model ibm quantum computer can outperform quantum annealers for nontrivial binary optimization problems, [arXiv](#) , [2406.01743](#).
- [17] S. A. Moses, C. H. Baldwin, M. S. Allman, R. Ancona, L. Ascarrunz, C. Barnes, J. Bartolotta, B. Bjork, P. Blanchard, M. Bohn, *et al.*, A race-track trapped-ion quantum processor, *Phys. Rev. X* **13**, 041052 (2023).
- [18] E. Pelofske, A. Bärttschi, and S. Eidenbenz, Short-depth qaoa circuits and quantum annealing on higher-order ising models, *npj Quantum Inf.* **10**, 30 (2024).
- [19] J. A. Montanez-Barrera and K. Michielsen, Towards a universal qaoa protocol: Evidence of quantum advantage in solving combinatorial optimization problems, [arXiv](#) , [2405.09169](#).
- [20] However, the effective problem sizes solved on quantum annealers are smaller than the number of physical qubits due to embedding overheads [? ].
- [21] J. Roffe, Quantum error correction: an introductory

- guide, *Contemp. Phys.* **60**, 226 (2019).
- [22] D. Bluvstein, S. J. Evered, A. A. Geim, S. H. Li, H. Zhou, T. Manovitz, S. Ebadi, M. Cain, M. Kalinowski, D. Hangleiter, *et al.*, Logical quantum processor based on reconfigurable atom arrays, *Nature* **626**, 58 (2024).
  - [23] G. Q. Ai, Suppressing quantum errors by scaling a surface code logical qubit, *Nature* **614**, 676 (2023).
  - [24] M. P. Da Silva, C. Ryan-Anderson, J. M. Bello-Rivas, A. Chernoguzov, J. M. Dreiling, C. Foltz, J. P. Gaebler, T. M. Gatterman, D. Hayes, N. Hewitt, *et al.*, Demonstration of logical qubits and repeated error correction with better-than-physical error rates, *arXiv* , 2404.02280.
  - [25] S. Krinner, N. Lacroix, A. Remm, A. Di Paolo, E. Genois, C. Leroux, C. Hellings, S. Lazar, F. Swiadek, J. Herrmann, *et al.*, Realizing repeated quantum error correction in a distance-three surface code, *Nature* **605**, 669 (2022).
  - [26] S. Bravyi, G. Smith, and J. A. Smolin, Trading classical and quantum computational resources, *Phys. Rev. X* **6**, 021043 (2016).
  - [27] T. Peng, A. W. Harrow, M. Ozols, and X. Wu, Simulating large quantum circuits on a small quantum computer, *Phys. Rev. Lett.* **125**, 150504 (2020).
  - [28] W. Tang, T. Tomesh, M. Suchara, J. Larson, and M. Martonosi, Cutqc: using small quantum computers for large quantum circuit evaluations, in *Proceedings of the 26th ACM International conference on architectural support for programming languages and operating systems (New York)* (2021) pp. 473–486.
  - [29] M. DeCross, E. Chertkov, M. Kohagen, and M. Foss-Feig, Qubit-reuse compilation with mid-circuit measurement and reset, *Phys. Rev. X* **13**, 041057 (2023).
  - [30] Y. Kim, A. Eddins, S. Anand, K. X. Wei, E. Van Den Berg, S. Rosenblatt, H. Nayfeh, Y. Wu, M. Zaletel, K. Temme, *et al.*, Evidence for the utility of quantum computing before fault tolerance, *Nature* **618**, 500 (2023).
  - [31] M. Bechtold, J. Barzen, F. Leymann, A. Mandl, J. Obst, F. Truger, and B. Weder, Investigating the effect of circuit cutting in qaoa for the maxcut problem on nisc devices, *Quantum Sci. Technol.* **8**, 045022 (2023).
  - [32] M. Dupont, B. Sundar, B. Evert, D. E. B. Neira, Z. Peng, S. Jeffrey, and M. J. Hodson, Quantum optimization for the maximum cut problem on a superconducting quantum computer, *arXiv* , 2404.17579.
  - [33] A. Angone, X. Liu, R. Shaydulin, and I. Safro, Hybrid quantum-classical multilevel approach for maximum cuts on graphs, in *2023 IEEE High Performance Extreme Computing Conference (HPEC)* (IEEE, 2023) pp. 1–7.
  - [34] B. Bach, J. Falla, and I. Safro, Mlqaoa: Graph learning accelerated hybrid quantum-classical multilevel qaoa, *arXiv* , 2404.14399.
  - [35] C.-Y. Liu and H.-S. Goan, Hybrid gate-based and annealing quantum computing for large-size ising problems, *arXiv* , 2208.03283.
  - [36] M. J. Rančić, Noisy intermediate-scale quantum computing algorithm for solving an n-vertex maxcut problem with  $\log(n)$  qubits, *Phys. Rev. Res.* **5**, L012021 (2023).
  - [37] Y. Chatterjee, E. Bourreau, and M. J. Rančić, Solving various np-hard problems using exponentially fewer qubits on a quantum computer, *arXiv* , 2301.06978.
  - [38] Y. Tene-Cohen, T. Kelman, O. Lev, and A. Makmal, A variational qubit-efficient maxcut heuristic algorithm, *arXiv* , 2308.10383.
  - [39] M. Sciorilli, L. Borges, T. L. Patti, D. García-Martín, G. Camilo, A. Anandkumar, and L. Aolita, Towards large-scale quantum optimization solvers with few qubits, *arXiv* , 2401.09421.
  - [40] T. L. Patti, J. Kossaifi, A. Anandkumar, and S. F. Yelin, Variational quantum optimization with multibasis encodings, *Phys. Rev. Res.* **4**, 033142 (2022).
  - [41] L. Bittel and M. Kliesch, Training variational quantum algorithms is np-hard, *Phys. Rev. Lett.* **127**, 120502 (2021).
  - [42] M. Larocca, S. Thanasilp, S. Wang, K. Sharma, J. Biamonte, P. J. Coles, L. Cincio, J. R. McClean, Z. Holmes, and M. Cerezo, A review of barren plateaus in variational quantum computing, *arXiv* , 2405.00781.
  - [43] E. Farhi, J. Goldstone, S. Gutmann, and L. Zhou, The quantum approximate optimization algorithm and the sherrington-kirkpatrick model at infinite size, *Quantum* **6**, 759 (2022).
  - [44] J. Wurtz and D. Lykov, The fixed angle conjecture for qaoa on regular maxcut graphs, *arXiv* , 2107.00677.
  - [45] J. Wurtz and P. Love, Maxcut quantum approximate optimization algorithm performance guarantees for  $p \leq 1$ , *Phys. Rev. A* **103**, 042612 (2021).
  - [46] J. Basso, E. Farhi, K. Marwaha, B. Villalonga, and L. Zhou, The quantum approximate optimization algorithm at high depth for maxcut on large-girth regular graphs and the sherrington-kirkpatrick model, in *17th Conference on the Theory of Quantum Computation, Communication and Cryptography (TQC 2022)* (2022) pp. 7:1–7:21.
  - [47] D. Sherrington and S. Kirkpatrick, Solvable model of a spin-glass, *Phys. Rev. Lett.* **35**, 1792 (1975).
  - [48] B. Y. L. Tan, M.-A. Lemonde, S. Thanasilp, J. Tangpanitanon, and D. G. Angelakis, Qubit-efficient encoding schemes for binary optimisation problems, *Quantum* **5**, 454 (2021).
  - [49] E. X. Huber, B. Y. L. Tan, P. R. Griffin, and D. G. Angelakis, Exponential qubit reduction in optimization for financial transaction settlement, *arXiv* , 2307.07193.
  - [50] I. D. Leonidas, A. Dukakis, B. Y. L. Tan, and D. G. Angelakis, Qubit efficient quantum algorithms for the vehicle routing problem on nisc processors, *arXiv* , 2306.08507.
  - [51] U. Azad, B. K. Behera, E. A. Ahmed, P. K. Panigrahi, and A. Farouk, Solving vehicle routing problem using quantum approximate optimization algorithm, *IEEE Trans. Intell. Transp. Syst.* , 7564 (2022).
  - [52] M. R. Perelshtein, A. I. Pakhomchik, A. A. Melnikov, M. Podobrii, A. Termanova, I. Kreidich, B. Nuriev, S. Iudin, C. W. Mansell, and V. M. Vinokur, Nisc-compatible approximate quantum algorithm for unconstrained and constrained discrete optimization, *Quantum* **7**, 1186 (2023).
  - [53] A. Lucas, Ising formulations of many np problems, *Front. Phys.* **2**, 5 (2014).
  - [54] See supplementary materials.
  - [55] D. J. Wales and J. P. K. Doye, Global optimization by basin-hopping and the lowest energy structures of lennard-jones clusters containing up to 110 atoms, *J. Phys. Chem. A* **101**, 5111 (1997).
  - [56] D. C. Liu and J. Nocedal, On the limited memory bfgs method for large scale optimization, *Math. Program.* **45**, 503 (1989).
  - [57] F. Glover, Z. Lü, and J.-K. Hao, Diversification-driven tabu search for unconstrained binary quadratic problems,

- 4OR **8**, 239 (2010).
- [58] I. Dunning, S. Gupta, and J. Silberholz, What works best when? a systematic evaluation of heuristics for max-cut and QUBO, *INFORMS Journal on Computing* **30**, 608 (2018).
  - [59] L. Zhou, S.-T. Wang, S. Choi, H. Pichler, and M. D. Lukin, Quantum approximate optimization algorithm: Performance, mechanism, and implementation on near-term devices, *Phys. Rev. X* **10**, 021067 (2020).
  - [60] J. Basso, E. Farhi, K. Marwaha, B. Villalonga, and L. Zhou, The quantum approximate optimization algorithm at high depth for maxcut on large-girth regular graphs and the sherrington-kirkpatrick model, *arXiv* , 2110.14206.
  - [61] A. Galda, E. Gupta, J. Falla, X. Liu, D. Lykov, Y. Alexeev, and I. Safro, Similarity-based parameter transferability in the quantum approximate optimization algorithm, *arXiv* , 2307.05420.
  - [62] L. T. Brady, C. L. Baldwin, A. Bapat, Y. Kharkov, and A. V. Gorshkov, Optimal protocols in quantum annealing and quantum approximate optimization algorithm problems, *Phys. Rev. Lett.* **126**, 070505 (2021).
  - [63] Y. Chen, L. Zhu, N. J. Mayhall, E. Barnes, and S. E. Economou, How much entanglement do quantum optimization algorithms require?, in *Quantum 2.0* (Optica Publishing Group, 2022) pp. QM4A–2.
  - [64] M. Dupont, N. Didier, M. J. Hodson, J. E. Moore, and M. J. Reagor, Entanglement perspective on the quantum approximate optimization algorithm, *Phys. Rev. A* **106**, 022423 (2022).
  - [65] A. C. Nakhil, T. Quella, and M. Usman, Calibrating the role of entanglement in variational quantum circuits, *Phys. Rev. A* **109**, 032413 (2024).
  - [66] G. Parisi, Infinite number of order parameters for spin-glasses, *Phys. Rev. Lett.* **43**, 1754 (1979).
  - [67] S. Boettcher, Extremal optimization for sherrington-kirkpatrick spin glasses, *Eur. Phys. J. B* **46**, 501 (2005).

# Supplementary Material for Qubit-efficient quantum combinatorial optimization solver

## QUBIT-EFFICIENT ENCODING

In the main text, we described the qubit-efficient encoding of  $N$  classical variables [Eq. (1)], and how to estimate  $\bar{z}_i$  and  $\bar{z}_i \bar{z}_j$  [Eqs. (2) and (3)]. Here, we exemplify these using the ( $N = 4$ ,  $d = 2$ ) case as an example.

Encoding  $N = 4$  variables using  $d = 2$  requires 3 qubits. The most generic 3-qubit wave function is

$$|\psi\rangle = c_0 |000\rangle + c_1 |001\rangle + \cdots + c_7 |111\rangle \quad (\text{S.1})$$

with  $\sum_{i=0}^7 |c_i|^2 = 1$ . Denoting the most significant bit as the label bit, projectively measuring this wave function gives the following measurements with respective probabilities,

Variables	Values	Probability
$(z_0, z_1)$	$(1, 1)$	$ c_0 ^2$
$(z_0, z_1)$	$(1, -1)$	$ c_1 ^2$
$(z_0, z_1)$	$(-1, 1)$	$ c_2 ^2$
$(z_0, z_1)$	$(-1, -1)$	$ c_3 ^2$
$(z_2, z_3)$	$(1, 1)$	$ c_4 ^2$
$(z_2, z_3)$	$(1, -1)$	$ c_5 ^2$
$(z_2, z_3)$	$(-1, 1)$	$ c_6 ^2$
$(z_2, z_3)$	$(-1, -1)$	$ c_7 ^2$

(S.2)

In an experiment with  $N_s$  shots,  $N_s^{(0)} \sim N_s \sum_{i=0}^3 |c_i|^2$  shots yield the values of  $(z_0, z_1)$ , and  $N_s^{(1)} \sim N_s \sum_{i=4}^7 |c_i|^2$  shots yield the values of  $(z_2, z_3)$ . The estimate for, e.g.,  $\bar{z}_0 \bar{z}_1$  if obtained from just the  $N_s^{(0)}$  shots as

$$\begin{aligned} \overline{z_0 z_1} &= \frac{\sum_{i,j=\pm 1} ij N(z_0 = i, z_1 = j)}{N_s^{(0)}} \\ &\sim \frac{N_s |c_0|^2 - |c_1|^2 - |c_2|^2 + |c_3|^2}{N_s (|c_0|^2 + |c_1|^2 + |c_2|^2 + |c_3|^2)} \end{aligned} \quad (\text{S.3})$$

where  $N(z_0 = i, z_1 = j)$  is the number of times  $(z_0, z_1)$  were measured as  $(i, j)$ . The expression in Eq. (S.3) is equal to  $\frac{\langle \hat{P}_{\ell=0} \hat{Z}_1 \hat{Z}_2 \rangle}{\langle \hat{P}_{\ell=0} \rangle}$ . Other correlations and one-body

terms can be similarly estimated as

$$\begin{aligned} \overline{z_0 z_1} &= \frac{|c_0|^2 - |c_1|^2 - |c_2|^2 + |c_3|^2}{|c_0|^2 + |c_1|^2 + |c_2|^2 + |c_3|^2} \\ \overline{z_2 z_3} &= \frac{|c_4|^2 - |c_5|^2 - |c_6|^2 + |c_7|^2}{|c_4|^2 + |c_5|^2 + |c_6|^2 + |c_7|^2} \\ \bar{z}_0 &= \frac{|c_0|^2 + |c_1|^2 - |c_2|^2 - |c_3|^2}{|c_0|^2 + |c_1|^2 + |c_2|^2 + |c_3|^2} \\ \bar{z}_1 &= \frac{|c_0|^2 - |c_1|^2 + |c_2|^2 - |c_3|^2}{|c_0|^2 + |c_1|^2 + |c_2|^2 + |c_3|^2} \\ \bar{z}_2 &= \frac{|c_4|^2 + |c_5|^2 - |c_6|^2 - |c_7|^2}{|c_4|^2 + |c_5|^2 + |c_6|^2 + |c_7|^2} \\ \bar{z}_3 &= \frac{|c_4|^2 - |c_5|^2 + |c_6|^2 - |c_7|^2}{|c_4|^2 + |c_5|^2 + |c_6|^2 + |c_7|^2} \end{aligned} \quad (\text{S.4})$$

The estimate for the cost  $C = \sum_{ij} w_{ij} z_i z_j$  is

$$\begin{aligned} C &= w_{12} \bar{z}_1 \bar{z}_2 + w_{34} \bar{z}_3 \bar{z}_4 \\ &\quad + w_{13} \bar{z}_1 \bar{z}_3 + w_{14} \bar{z}_1 \bar{z}_4 + w_{23} \bar{z}_2 \bar{z}_3 + w_{24} \bar{z}_2 \bar{z}_4. \end{aligned} \quad (\text{S.5})$$

## d=N

In the  $d = N$  case, there are no label bits, and each variable is mapped one-to-one with a data bit. This is the usual way variables are mapped to qubits. Correlations  $z_i z_j$  are, e.g., estimated as  $\bar{z}_i \bar{z}_j = \langle \hat{Z}_i \hat{Z}_j \rangle$ , and  $C = \sum_{ij} w_{ij} z_i z_j$  is  $C = \langle \hat{H} \rangle$  with  $\hat{H} = \sum_{ij} w_{ij} \hat{Z}_i \hat{Z}_j$ .

## d=1

In the  $d = 1$  case, there are  $\log_2 N$  label bits, and all the variables are mapped to one data bit. All correlations  $z_i z_j$  are estimated as  $\bar{z}_i \bar{z}_j = \bar{z}_i \times \bar{z}_j$ .

## d=2

The  $d = 2$  case, coincidentally, requires the same number of qubits as  $d = 1$ . However, the mappings between qubits and variables are different. For  $d = 2$ , there are  $\log_2 N - 1$  label bits and 2 data bits, unlike the  $d = 1$  case.

## ENTANGLEMENT IN THE QUBIT-EFFICIENT ENCODING

Entanglement is an essential property of quantum devices and algorithms, and is the reason for non-simulability and potential utility of quantum optimization. The growth of entanglement induced by the QAOA



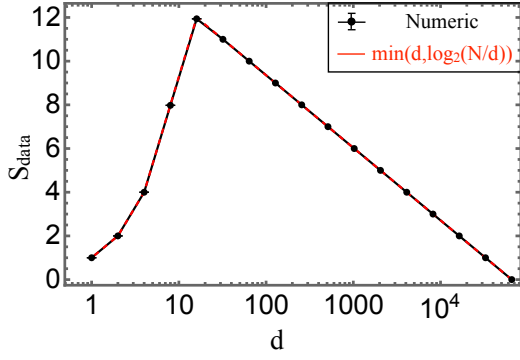


FIG. S.1. Average entanglement entropy of the data qubits that store bit strings of length  $N = 2^{16}$ . The data qubits have volume law entanglement.

circuit has been previously studied [63–65], finding for example volume-law entanglement in the wave function between the initial and final state. The target state of QAOA is a product state with no entanglement.

In the qubit-efficient approach, however, the target state is not a product state. Instead, the bit string solution  $\mathbf{z}$  is stored as the entangled wave function  $|\phi(\mathbf{z})\rangle = \sum_{\ell} \lambda_{\ell} |\ell\rangle \otimes |\mathbf{z}_{\ell}\rangle$  [Eq. (1) in the main text].  $\mathbf{z}_{\ell}$  are length- $d$  subsets of  $\mathbf{z}$ , where the subscript  $\ell$  runs from 0 to  $N/d-1$ . Here, we quantify the entanglement present in the target wave function by calculating the entanglement entropy of the data qubits.

The reduced density matrix for the data qubits, obtained by tracing over the label qubits, is

$$\rho_{\text{data}} = \sum_{\ell=0}^{N/d-1} |\lambda_{\ell}|^2 |\mathbf{z}_{\ell}\rangle \langle \mathbf{z}_{\ell}|, \quad (\text{S.6})$$

and its von Neumann entropy is  $S_{\text{data}} = -\text{Tr}(\rho_{\text{data}} \log_2 \rho_{\text{data}})$ .

Figure S.1 plots the average entanglement entropy, averaged over 100 random bit strings of length  $N = 2^{16}$ , versus  $d$ , assuming wave functions with uniform  $|\lambda_{\ell}|^2 = d/N$ . Two regimes emerge. When  $d \lesssim 16$ , the entanglement entropy increases as  $d$ , whereas for  $d \gtrsim 16$ , it decreases as  $\log_2(N/d)$ . This entropy is the smaller of the number of data and label qubits, indicating volume law entanglement.

We can understand the two regimes as follows. When we encode a random bit string  $\mathbf{z}$  at large  $d$ , i.e.  $2^d \gg N/d$ , the probability that any two  $\mathbf{z}_{\ell}$  are equal is exponentially small in  $d$ , therefore on average,  $S_{\text{data}} = -\sum_{\ell=0}^{N/d-1} |\lambda_{\ell}|^2 \log_2 |\lambda_{\ell}|^2$ . For uniform  $|\lambda_{\ell}|^2 = d/N$ , the entropy reduces to  $S_{\text{data}} = \log_2(N/d)$ .

When  $2^d \ll N/d$ , there is a significant probability that there will be repetitions among the different  $\mathbf{z}_{\ell}$ . The average number of times any  $\mathbf{z}_{\ell}$  would be repeated in  $\mathbf{z}$  is  $\frac{N/d}{2^d}$ . Those repetitions must be grouped together in  $\rho_{\text{data}}$ . For uniform  $|\lambda_{\ell}|^2 = d/N$ , this gives  $\rho_{\text{data}} \sim \sum_{\ell=0}^{2^d-1} \frac{d}{N} \frac{N/d}{2^d} |\mathbf{z}_{\ell}\rangle \langle \mathbf{z}_{\ell}|$ . The entropy of this state

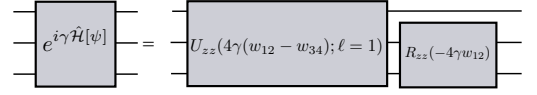


FIG. S.2. Simplification of the phase separator term in the ansatz. Implementation of these logical gates in terms of hardware-native gates are given in Fig. S.3

is  $S_{\text{data}} = d$ .

## EXAMPLE PROBLEM IN FIG. 2

In the main text, we exemplified the qubit-efficient encoding [Eq. (1)] and the ansatz using an SK problem with  $N = 4$  variables. Here, we discuss this example in detail.

### Example problem

The specific problem considered in Fig. 1 in the main text has the weights

$$w = \begin{pmatrix} 0 & 1 & -1 & 1 \\ 1 & 0 & -1 & -1 \\ -1 & -1 & 0 & 1 \\ 1 & -1 & 1 & 0 \end{pmatrix}. \quad (\text{S.7})$$

It can be verified, e.g. by explicitly enumerating all the 16 bitstrings for the 4 variables, that the ground state solutions for this example are  $\mathbf{z}^* = (1, -1, 1, -1)$  and  $-\mathbf{z}^* = (-1, 1, -1, 1)$ , with the ground state cost  $C^* = -4$ . These solutions can be represented by the respective wave functions  $|\phi(\mathbf{z}^*)\rangle = (|0\rangle_{\text{label}} \otimes |01\rangle_{\text{data}} + |1\rangle_{\text{label}} \otimes |01\rangle_{\text{data}})/\sqrt{2}$  and  $|\phi(-\mathbf{z}^*)\rangle = (|0\rangle_{\text{label}} \otimes |10\rangle_{\text{data}} + |1\rangle_{\text{label}} \otimes |10\rangle_{\text{data}})/\sqrt{2}$  at  $d = 2$ .

To implement the ansatz  $|\psi_{p=1}\rangle = e^{-i\beta \hat{H}_x/2} e^{-i\gamma \hat{H}[\psi_0]/2} |\psi_0\rangle$ , we first need to determine  $\hat{H}[\psi_0]$ , where  $|\psi_0\rangle$  is the equal superposition state of 3 qubits. Measurements of  $|\psi_0\rangle$  would give

$$\begin{aligned} \bar{z}_1 = \bar{z}_2 = \bar{z}_3 = \bar{z}_4 &= 0, \\ \langle \psi_0 | \hat{P}_{\ell=0} \psi_0 \rangle &= \langle \psi_0 | \hat{P}_{\ell=1} \psi_0 \rangle = 1/2, \\ \Rightarrow \hat{H}[\psi_0] &= 2(w_{12} \hat{P}_{\ell=0} \hat{Z}_{d_1} \hat{Z}_{d_2} + w_{34} \hat{P}_{\ell=1} \hat{Z}_{d_1} \hat{Z}_{d_2}). \end{aligned} \quad (\text{S.8})$$

Next, we describe how to implement the ansatz at arbitrary  $p$ , which can be straightforwardly specialized to  $p = 1$ .

### Circuit compilation of the ansatz

Here, we describe how to implement the ansatz  $|\psi_p\rangle = e^{i\beta \hat{H}_x} e^{i\gamma \hat{H}[\psi_{p-1}]} |\psi_{p-1}\rangle$  for the specific case of  $N = 4, d =$

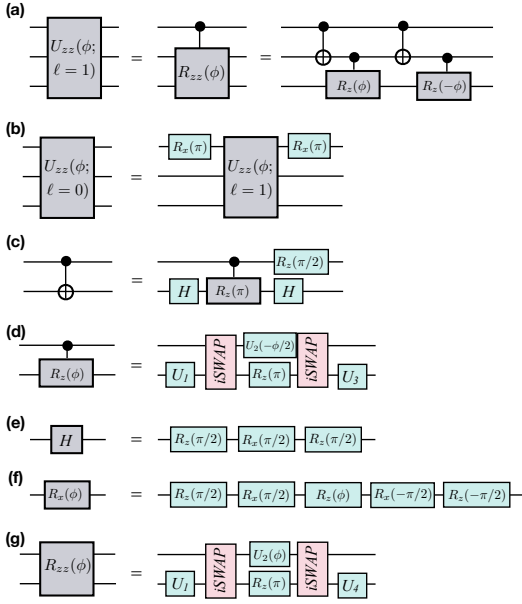


FIG. S.3. Compilation of common gates in terms of gates native to Rigetti's Ankaa™-9Q-3.

2 considered here. A general implementation of the ansatz for arbitrary  $N$  and  $d$  is discussed later.

Figure S.2 breaks down  $e^{i\gamma\mathcal{H}[\psi_{p-1}]/2}$  into a 3-qubit gate and 2-qubit gate. Figure S.3 shows how to implement compile these gates into the native gates on Rigetti's Ankaa™-9Q-3 chip,  $R_x(\pi/2) \equiv \exp(-i\hat{X}\pi/4)$  and  $i\text{SWAP} = \exp(i\pi/4(\hat{X}\otimes\hat{X} + \hat{Y}\otimes\hat{Y}))$ .  $R_z(\phi)$  gates are virtually applied via frame tracking. The unitary  $e^{i\beta\mathcal{H}_x}$  can be implemented with  $R_x(-2\beta)$  on all the qubits. In Fig. S.3,

$$\begin{aligned} U_1 &= R_x(-\pi/2) \\ U_2(\phi) &= R_z(\pi/2)R_x(\pi/2)R_z(\phi)R_x(-\pi/2) \\ U_3 &= R_z((\pi + \phi)/2)R_x(\pi/2) \\ U_4 &= R_z(\pi/2)R_x(\pi/2) \end{aligned} \quad (\text{S.9})$$

#### Optimization of the ansatz at $p=1$

After implementing the ansatz  $|\psi_{p=1}\rangle = e^{i\beta_1\mathcal{H}_x}e^{i\gamma_1\mathcal{H}[\psi_0]}|\psi_0\rangle$ , explicit calculation of the expectation value of the cost gives

$$\begin{aligned} C[\psi_{p=1}] &= (w_{12} - w_{34}) \sin 2\beta_1 (\sin(4\gamma_1 w_{12}) - \sin(4w_{34}\gamma_1) + \sin(2\gamma_1(w_{12} - w_{34}))) \\ &\quad + \sin 2\beta_1 \cos 2\beta_1 (w_{12} + w_{34}) (\sin(4w_{12}\gamma_1) + \sin(4w_{34}\gamma_1)). \end{aligned} \quad (\text{S.10})$$

For the specific example in Eq. (S.7), the noiseless cost is  $C[\psi_{p=1}] = 2 \sin 4\beta_1 \sin 4\gamma_1$ . The cost measured on Ankaa™-9Q-3 as well as numerically computed from 10000 shots of a noiseless simulation, plotted in Figs. 2(b-c) in the main text, closely match this expression, with the former having an overall reduction in magnitude attributable to hardware noise.

The parameters which minimize the cost at  $p = 1$  are  $(\beta_1, \gamma_1) = (\frac{3\pi}{8}, \frac{\pi}{8})$ , and the wave function  $|\psi_{p=1}\rangle$  is

$$\begin{aligned} |\psi_{p=1}\rangle &= \frac{(|0\rangle_{\text{label}} + |1\rangle_{\text{label}}) \otimes (|01\rangle_{\text{data}} + |10\rangle_{\text{data}})}{2} \\ &= \frac{|\phi(\mathbf{z}^*)\rangle + |\phi(-\mathbf{z}^*)\rangle}{\sqrt{2}}. \end{aligned} \quad (\text{S.11})$$

The wave function is an equal superposition of  $|\phi(\mathbf{z}^*)\rangle$  and  $|\phi(-\mathbf{z}^*)\rangle$  due to  $\mathbb{Z}_2$  symmetry of the ansatz. Figure S.4 plots the distribution of bit strings sampled from this wave function (magenta), and measured in executing the ansatz on Rigetti's Ankaa™-9Q-3 chip. The ideal wave function gives

$$\begin{aligned} \bar{z}_1 \bar{z}_2 &= \bar{z}_3 \bar{z}_4 = -1, \\ \bar{z}_1 &= \bar{z}_2 = \bar{z}_3 = \bar{z}_4 = 0, \end{aligned} \quad (\text{S.12})$$

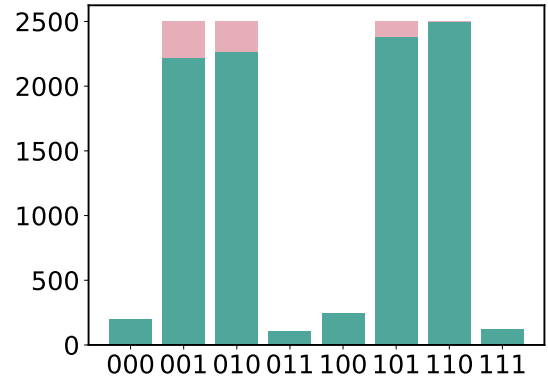


FIG. S.4. Distribution of bit strings measured on Rigetti's Ankaa™-9Q-3 chip (teal), and predicted from the wave function (magenta), at the optimal angles of the ansatz for the example in Fig. 2 in the main text.

therefore the cost is  $C[\psi_{p=1}] = -(w_{12} + w_{34}) = -2$ . The measured cost on Rigetti's Ankaa™-9Q-3 is  $C = -1.736(1)$ . We remark on the unique feature of the qubit-

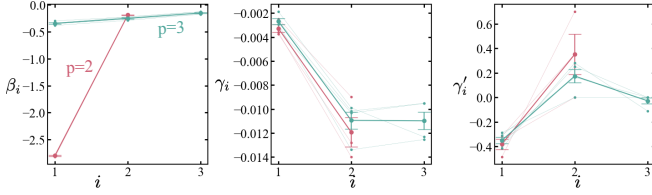


FIG. S.5. Optimal parameters returned by the classical optimizer for the five SK problem instances with  $N = 64$  variables in Fig. 3 in the main text, at  $d = 4$ . The thin curves plot the instance-by-instance optimal parameters, and the thick curves plot their mean values. We find the curves are clustered together.

efficient encoding that a *superposition* of ground state solutions does not have the same cost  $C$  as the ground state cost  $C^*$ , whereas the cost for the superposition would be equal to the ground state cost  $C^*$  in the  $d = N$  case. This is because  $\bar{z}_i = 0$ , therefore several terms in the cost at  $d < N$  are 0. Therefore, explicitly breaking the  $\mathbb{Z}_2$  symmetry in the ansatz is necessary. We broke the symmetry with the one-body bias term,  $\exp(i\gamma'\hat{\mathcal{H}}_z)$ .

#### PARAMETER CLUSTERING IN THE SK MODEL AND THE QUBIT-EFFICIENT ANSATZ

Previous works [43, 46] have found evidence of parameter clustering when solving SK problem instances using QAOA (which is the  $d = N$  limit of our ansatz). Optimal parameters and approximation ratios for the typical problem instance have been tabulated up to  $p = 12$ . Our cost function  $C$  is related to the cost  $\tilde{C}$  in Ref. [43] via  $C = \sqrt{N}\tilde{C}$ , and our parameters  $(\beta, \gamma)$  at  $d = N$  are related to parameters  $(\tilde{\beta}, \tilde{\gamma})$  in Ref. [43] via  $\beta = -\tilde{\beta}$  and  $\gamma = -\tilde{\gamma}/\sqrt{N}$ . The minus sign is irrelevant since  $C$  is real. The optimal value of  $\gamma$ , in our convention, scales as  $1/\sqrt{N}$ . The optimal values of  $(\beta, \gamma)$  and  $C$  up to  $p = 11$  are the same for two classes of SK models –  $w_{ij} \in \{\pm 1\}$ , and  $w_{ij} \sim \mathcal{N}(0, 1)$ .

We showed numerical evidence in Fig. 4 in the main text that parameter clustering occurs for the qubit-efficient encoding ansatz ( $d < N$ ) as well. Figure S.5 plots the optimal parameters found by the classical optimizer for the 5 problem instances in Fig. 3, up to  $p = 3$  at  $d = 4$  and  $N = 64$ . While Ref. [43] did not have – nor require (see previous section) –  $\gamma'$ , we introduced one-body bias terms  $\gamma'\hat{\mathcal{H}}_z$  to break  $\mathbb{Z}_2$  symmetry. We find that the thin curves, which plot the optimal parameters for the 5 instances, are clustered together. We also find that the optimal values of  $\gamma$  are smaller than those of  $\beta$  and  $\gamma'$ .

We hypothesize that the optimal coefficient multiplying  $\hat{Z}_i\hat{Z}_j$  in the qubit-efficient ansatz scales  $\propto 1/\sqrt{N}$ , just like in the  $d = N$  case. We validate this hypothesis as follows. Ising terms such as  $\hat{Z}_i\hat{Z}_j$  appear in the

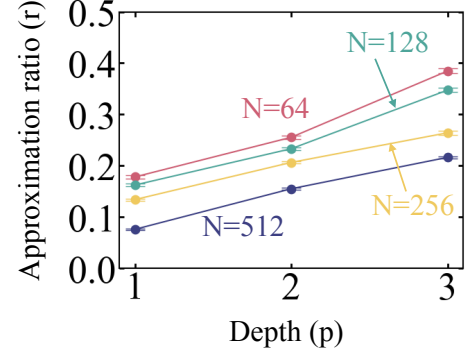


FIG. S.6. Average approximation ratios for optimized parameters for 100 SK problem instances at different sizes and  $d = 4$ , where the same parameters were used for all the instances.

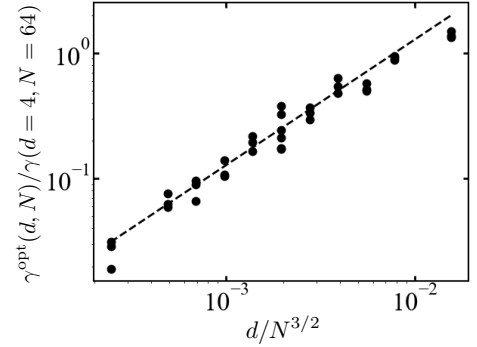


FIG. S.7. Optimal ratios  $\gamma^{\text{opt}}(N, d; p, i)/\gamma(N = 64, d = 64; p, i)$  scale as  $d/N^{3/2}$ . The points include  $1 \leq p \leq 3$ ,  $N \in \{64, 128, 256\}$ ,  $d \in \{1, 2, 4, 8\}$ , with one SK problem instance at each  $N$  and  $d$ . Dashed line plots  $d/N^{3/2}$  as guide to the eye.

ansatz via  $\gamma \frac{\hat{P}_\ell \hat{Z}_{d_i} \hat{Z}_{d_j}}{\langle \hat{P}_\ell \rangle}$ . Here,  $\langle \hat{P}_\ell \rangle = d/N$  in the equal superposition state which is the  $p = 0$  state of the ansatz, although it will vary with  $p$ . Setting  $\gamma \frac{N}{d} \propto 1/\sqrt{N}$  gives  $\gamma(N, d) \propto 1/N^{3/2}$ . This is the rescaling we applied when we used optimal parameters from  $N = 64$  to solve SK problems instances with  $N = 128$  in Fig. 3(c), i.e.  $\gamma^*(N = 128, d = 4) = \gamma^*(N = 64, d = 4)/2^{3/2}$ . We perform the same rescaling and calculate the approximation ratios for an ensemble of 100 SK problem instances with  $N = 256, 512$  in Fig. S.6, and find the approximation ratio increases with  $p$ .

Further, we validate the scaling of  $\gamma$  with the following optimization procedure. For an ensemble of SK problems at different sizes and  $d$ , we fix the values of  $\beta(N, d; p, i)$  and  $\gamma'(N, d; p, i)$  from one instance at  $N = 64, d = 4$ , and vary the values of  $\gamma(N, d; p, i)$ , where  $1 \leq i \leq p$ . We assume that  $\gamma(N, d; p, i)/\gamma(N = 64, d = 4; p, i) = \theta(N, d; p)$  is a constant, and optimize over  $\theta(N, d; p)$ . Figure S.7 finds that  $\theta^{\text{opt}}(N, d; p) \propto d/N^{3/2}$ , as predicted by the above argument.

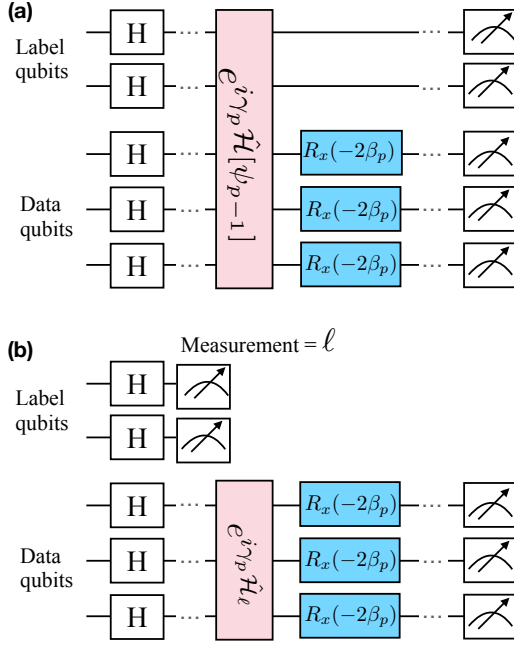


FIG. S.8. An ansatz with phase separators and one-qubit rotations on data qubits only. Executing the ansatz in (a) is equivalent to repeating the ansatz in (b) for  $\ell = 0 \dots (N/d - 1)$ , and reduces to implementing QAOA on the groups with  $d$  variables each.

### BASLINE PERFORMANCE OF A RELATED ANSATZ

Here, we consider a slightly modified ansatz given in Fig. S.8(a). The difference with the ansatz in the main text is that there are no  $R_x$  rotations of the label bits. Figure S.8(a) can be simplified to the ansatz in Fig. S.8(b). This simplification uses the identity that applying a controlled gate – apply  $U$  on target bits if control bits' value is  $x$  – followed by a measurement of the control bits is equivalent to first doing a measurement on the control bits and then implementing  $U$  on the target bits if the measurement is  $x$ . The ansatz in Fig. S.8(b) essentially implements the QAOA ansatz on  $d$  data bits using the SK problem weights on the subset of the  $d$  variables corresponding to the measured label value. Repeating the ansatz in Fig. S.8(b) several times essentially solves all the  $d$ -variable subproblems with label  $\ell$ , obtains the cost  $C_\ell$  for the subproblems  $\ell = 0 \dots (N/d - 1)$ , and returns the final cost,

$$C = \sum_{\ell=0}^{N/d-1} C_\ell. \quad (\text{S.13})$$

When the size of the problem being solved by QAOA is large, Ref. [43] predicts clustering of QAOA parameters and tabulates the approximation ratio,  $r^*(p)$  up to  $p = 11$ . The asymptotic value of the ground state cost for  $N$  variables is  $C_{\text{asympt.}}^*(N) = -PN^{3/2} + \alpha N^\omega$ ,

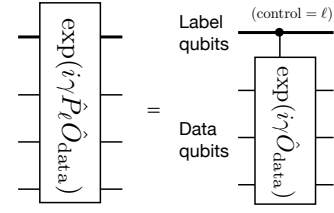


FIG. S.9. The phase separator unitary in the ansatz [Eq.(6) in the main text] is equivalent to implementing controlled unitaries with control as label qubits, and targets as Ising interactions on the data qubits.

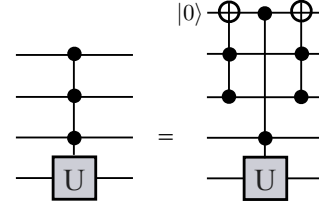


FIG. S.10. Reduction of controlled-unitary with  $m$  control bits to a controlled-unitary with  $(m - 1)$  control bits and one ancilla bit. This simplification, along with the compilation of the Toffoli gate in (b), can be recursively used to reduce the controlled-unitary in Fig. S.9 to hardware-native gates.

where  $P \approx 0.7632$  is the Parisi constant [66],  $\omega = 5/6$  and  $\alpha \approx 0.7$  is a non-universal constant that accounts for finite-size effects [67]. Similarly, for  $d \gg 1$ , the ground state cost for the subproblems with  $d$  variables is  $C_{\text{asympt.}}^*(d) \sim -Pd^{3/2}$ , neglecting the subleading term, and the ansatz in Fig. S.8 at  $p$  layers yields  $C_\ell^*(p) = r^*(p) \times Pd^{3/2}$ . Then, the total cost for  $N$  variables is

$$C^* = r^*(p) \times Pd^{3/2} \times \frac{N}{d}. \quad (\text{S.14})$$

The approximation ratio for this ansatz is

$$r^* \equiv C^*/C_{\text{asympt.}}^*(N) \sim r^*(p) \times \sqrt{\frac{d}{N}}. \quad (\text{S.15})$$

This approximation ratio is plotted as the black dash-dotted lines in Fig. 4.



## CIRCUIT IMPLEMENTATION OF THE ANSATZ

### Phase separator unitary

The phase separator Hamiltonian [Eq.(5)] in the main text is

$$\begin{aligned} \hat{\mathcal{H}}[\psi] = & \sum_{\substack{i < j \\ \ell_i = \ell_j}} w_{ij} \frac{\hat{P}_{\ell_i} \hat{Z}_{d_i} \hat{Z}_{d_j}}{\langle \psi | \hat{P}_{\ell_i} | \psi \rangle} \\ & + \frac{1}{2} \sum_{\substack{i < j \\ \ell_i = \ell_j}} w_{ij} \left( \bar{z}_i \frac{\hat{P}_{\ell_j} \hat{Z}_{d_j}}{\langle \psi | \hat{P}_{\ell_j} | \psi \rangle} + \bar{z}_j \frac{\hat{P}_{\ell_i} \hat{Z}_{d_i}}{\langle \psi | \hat{P}_{\ell_i} | \psi \rangle} \right). \end{aligned} \quad (\text{S.16})$$

Since all the terms in  $\hat{\mathcal{H}}[\psi]$  commute with each other, the unitary  $\exp(i\gamma\hat{\mathcal{H}}[\psi])$  is a product of a unitary due to each term. The unitary due to each term is of the form  $\exp(i\gamma\hat{P}_\ell\hat{O}_{\text{data}})$  where  $\hat{O}_{\text{data}} = \hat{Z}_{d_i}$  or  $\hat{O}_{\text{data}} = \hat{Z}_{d_i}\hat{Z}_{d_j}$ .

When the label qubits are in the state  $|\ell\rangle$ , the projection operator  $\hat{P}_\ell$  is 1, therefore  $\exp(i\gamma\hat{P}_\ell\hat{O}_{\text{data}})$  implements  $\exp(i\gamma\hat{O}_{\text{data}})$  on the data qubits. When the label qubits are in  $|\ell' \neq \ell\rangle$ , the projection operator  $\hat{P}_\ell$  is 0, therefore  $\exp(i\gamma\hat{P}_\ell\hat{O}_{\text{data}})$  does nothing. This is nothing but a controlled-unitary operator, which implements the target unitary  $\exp(i\gamma\hat{O}_{\text{data}})$  if the label qubits are in  $|\ell\rangle$ , as depicted in Fig. S.9. One method to implement controlled unitaries with many control bits is shown in Fig. S.10(a).

### SHOT NOISE

In Fig. 3 of the main text, we variationally optimized the cost computed from a noiseless calculation of the wave function using a state vector simulator. In Figs. S.11 and S.12, we show that the estimated cost converges to the exact cost from the wave function at  $O(1000)$  shots for  $N = 64$  and  $128$ .

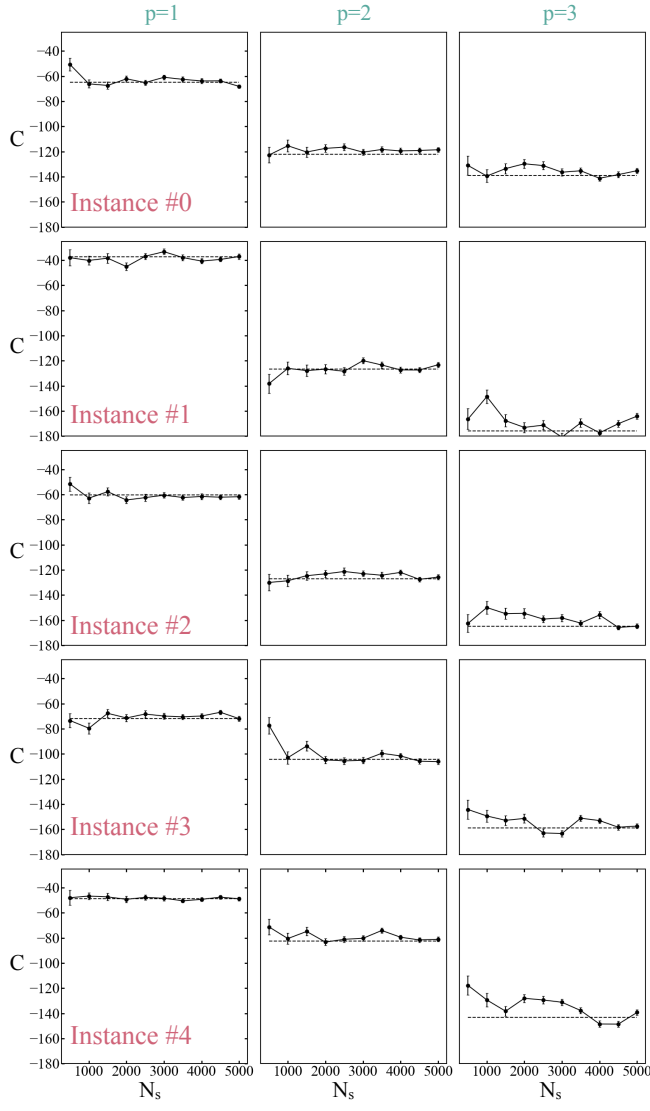


FIG. S.11. Estimated cost versus number of shots for the 5 SK problem instances in Fig. 3 of the main text at  $N = 64, d = 4$ . The costs converge to the exact cost computed from the wave function (dashed line) at  $\sim 1000$  shots.

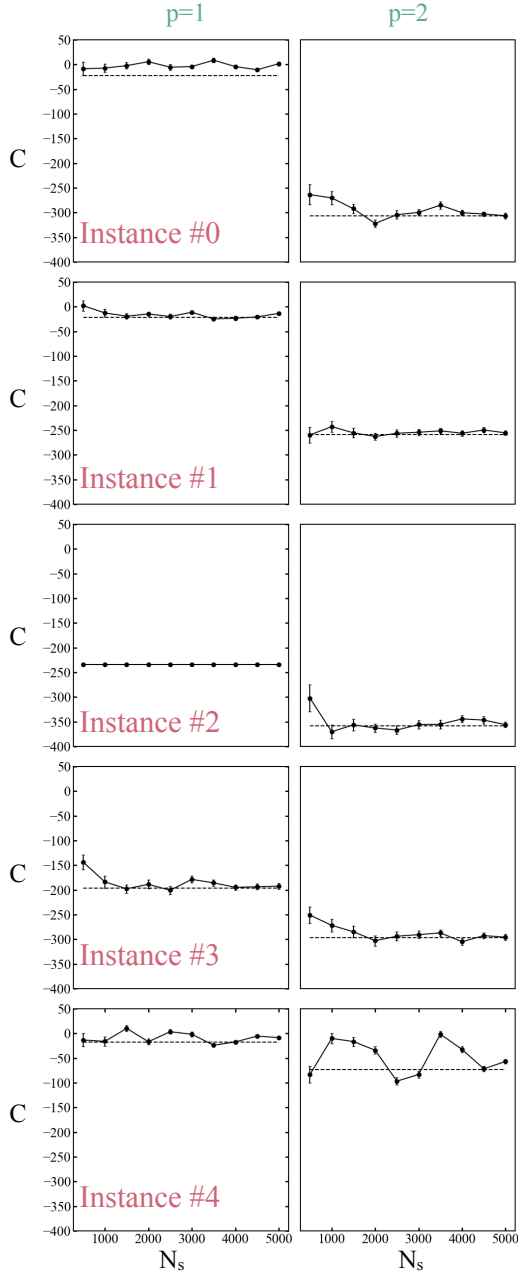


FIG. S.12. Estimated cost versus number of shots for the 5 SK problem instances in Fig. 3 of the main text at  $N = 128, d = 4$ . The costs converge to the exact cost computed from the wave function (dashed line) at  $O(1000)$  shots.